Chapter 9
Transient Chaos in Spatially Extended Systems

Chaos is not restricted to systems without any spatial extension: it in fact occurs commonly in spatially extended dynamical systems that are most typically described by nonlinear partial differential equations (PDEs). If the patterns generated by such a system change randomly in time, we speak of spatiotemporal chaos, a kind of temporally chaotic pattern-forming process. If, in addition, the patterns are also spatially irregular, there is fully developed spatiotemporal chaos. In principle, the phase-space dimension of a spatially extended dynamical system is infinite. However, in practice, when a spatial discretization scheme is used to solve the PDE, or when measurements are made in a physical experiment with finite spatial resolution, the effective dimension of the phase space is not infinite but still high.

Transient chaos is common in dissipative spatiotemporal systems. The basic reason is that spatial coupling is typically diffusive. The asymptotic attractors are therefore often temporally periodic, or even time-independent. It is the approach toward these attractors that is chaotic. In this sense, spatiotemporal chaos often collapses after some time, and a regular behavior then takes over. If the lifetime increases rapidly with the system size, the transients are *supertransients*. An important physical context in which supertransients arise is fluid dynamical turbulence in pipe flows, where the well-known stationary laminar solution is the only asymptotic attractor, and the observed turbulent behavior appears to be a kind of transient chaos only. Motivated by this example, we shall sometimes call the fully developed chaotic behavior of other spatiotemporal systems "turbulent."

In systems exhibiting supertransients, a general picture emerges: In a large system, it is not possible to determine whether the observed "turbulence" is transient unless an asymptotic time regime is reached. If the transient time is much longer than any physically realizable time, the system is effectively "turbulent," regardless of the nature of the asymptotic attractor. The transients mask in this case the real attractor, and pose a fundamental difficulty for observing the asymptotic state of the system. In this sense, attractors are irrelevant to "turbulence." Supertransients are thus perhaps the most surprising applications of the concept of transient chaos to high-dimensional dynamical systems.

In this chapter, we first introduce several paradigmatic models of spatially extended dynamical systems and discuss supertransients in different models. Scaling laws with the system size are derived. We then address the effect of noise

Y.-C. Lai and T. Tél, *Transient Chaos: Complex Dynamics on Finite-Time Scales*, Applied Mathematical Sciences 173, DOI 10.1007/978-1-4419-6987-3_9,

and of nonlocal couplings on supertransients, discuss various crisis phenomena in spatially extended systems, and characterize the fractal properties of supertransients. Finally, turbulence in pipe flows, which represents an important physical situation in which supertransients can be observed experimentally, is discussed.

9.1 Basic Characteristics of Spatiotemporal Chaos

9.1.1 Paradigmatic Models

There are several classes of models of spatially extended systems that can be used to study transient spatiotemporal chaos [775].

Coupled map lattices (CML), introduced by Kaneko [378], provide the simplest models for spatiotemporal dynamics of continuous variables. In a CML, the local building blocks of the dynamics are in the form of low-dimensional maps, and they are coupled to their neighbors according to some rule with a coupling of strength ε. In this model, both time and space are discrete, but the dynamical variables are continuous. The dynamics does depend on the boundary conditions. Often periodic boundary conditions are assumed, but absorbing boundary conditions have also been used. In one dimension, the typical form of a CML defined on N sites with diffusive local coupling is

$$x_{n+1}^i = (1-\varepsilon) f(x_n^i) + \frac{\varepsilon}{2}\left[f(x_n^{i+1}) + f(x_n^{i-1})\right], \quad i = 0, \ldots, N-1, \tag{9.1}$$

where x is the dynamical variable, $f(x)$ is a map describing the local dynamics, and n and i denote discrete time and space, respectively. For periodic boundary conditions we have $x_n^0 = x_n^{N-1}$, while for absorbing boundary conditions we have $x_n^0 = x_n^{N-1} = 0$ for any time instant n. The size of the system is N.

In a *cellular automaton* (CA) [833] even the dynamical variable is discrete. By coarsening the x variable of a CML, the dynamics is mapped onto that of a CA [609]. If, for example, the new variable is chosen to be 0 (1) for x smaller (larger) than a threshold, a two-state CA is obtained from (9.1).

The Kuramoto–Shivashinsky (KS) equation is a simple PDE exhibiting interesting spatiotemporal dynamics. It was derived to describe propagating patterns in plasmas, in chemistry and in cellular flames [85]. The KS equation governs the dynamics of a continuous scalar field $u(x,t)$ according to a nonlinear equation whose dimensionless form can be written as

$$\frac{\partial u}{\partial t} = -u\frac{\partial u}{\partial x} - \frac{\partial^2 u}{\partial x^2} - \frac{\partial^4 u}{\partial x^4}. \tag{9.2}$$

It is remarkable that there are no free parameters in the model, and hence the system size L serves as the only control parameter. Alternatively, one can fix the size and, after appropriate rescaling, convert (9.2) to

$$\frac{\partial u}{\partial t} = -u\frac{\partial u}{\partial x} - \frac{\partial^2 u}{\partial x^2} - \nu\frac{\partial^4 u}{\partial x^4}, \tag{9.3}$$

where $\nu \sim L^{-2}$ is a dimensionless parameter.

The complex Ginzburg–Landau (cGL) equation governs the spatiotemporal evolution of a complex field $\psi(\mathbf{r},t)$. It is the normal form of spatiotemporal systems in the vicinity of Hopf bifurcations [85]. In its most commonly used two-dimensional version, the cGL equation is

$$\frac{\partial \psi}{\partial t} = \mu\psi - (1+i\alpha)\Delta\psi + (1+i\beta)|\psi|^2\psi, \tag{9.4}$$

where Δ denotes the Laplacian. The system has three dimensionless parameters: μ, α, and β. When the dimensionless system size is fixed, the parameter μ characterizes the size dependence.

Reaction–diffusion (RD) equations describe the coupled dynamics of chemical concentrations, or interacting populations. Their general form for two concentrations $a(\mathbf{r},t)$ and $b(\mathbf{r},t)$ is

$$\frac{\partial a}{\partial t} = r_a(a,b) + \Delta a, \quad \frac{\partial b}{\partial t} = r_b(a,b) + \delta\Delta b, \tag{9.5}$$

where the functions r_a, r_b govern the nonlinear reaction equations in the homogeneous case, and the dimensionless parameter

$$\delta = D_b/D_a$$

is the ratio of the diffusion coefficients.

The Navier–Stokes (NS) equation describes the dynamics of the velocity and the pressure fields, $\mathbf{v}(\mathbf{r},\mathbf{t})$ and $p(\mathbf{r},t)$, respectively, of a viscous fluid. For incompressible flows not subject to any external force the dimensionless form of the NS equation is

$$\frac{\partial \mathbf{v}}{\partial t} + \mathbf{v}\nabla\mathbf{v} = -\nabla p + \frac{1}{Re}\Delta\mathbf{v}, \quad \nabla\cdot\mathbf{v} = 0, \tag{9.6}$$

where *Re* is the Reynolds number. Note that there is no dynamical equation for the pressure. It is the incompressibility equation $\nabla\cdot\mathbf{v} = 0$ that provides a condition of self-consistency to make the pressure unique.

Figure 9.1 presents several typical complex patterns in spatiotemporal systems.

9.1.2 Phase Spaces of Spatiotemporal Systems

The phase space of a spatiotemporal system is high-dimensional. In a CML, it is spanned by all the variables x^i at different sites $i = 0,\ldots,N-1$. In a system described by nonlinear PDEs, the infinite-dimensional phase space is spanned by the set of all possible spatial distributions of the fields, compatible with a given boundary condition. In the KS and cGL equations, these are the functional spaces $u(x)$

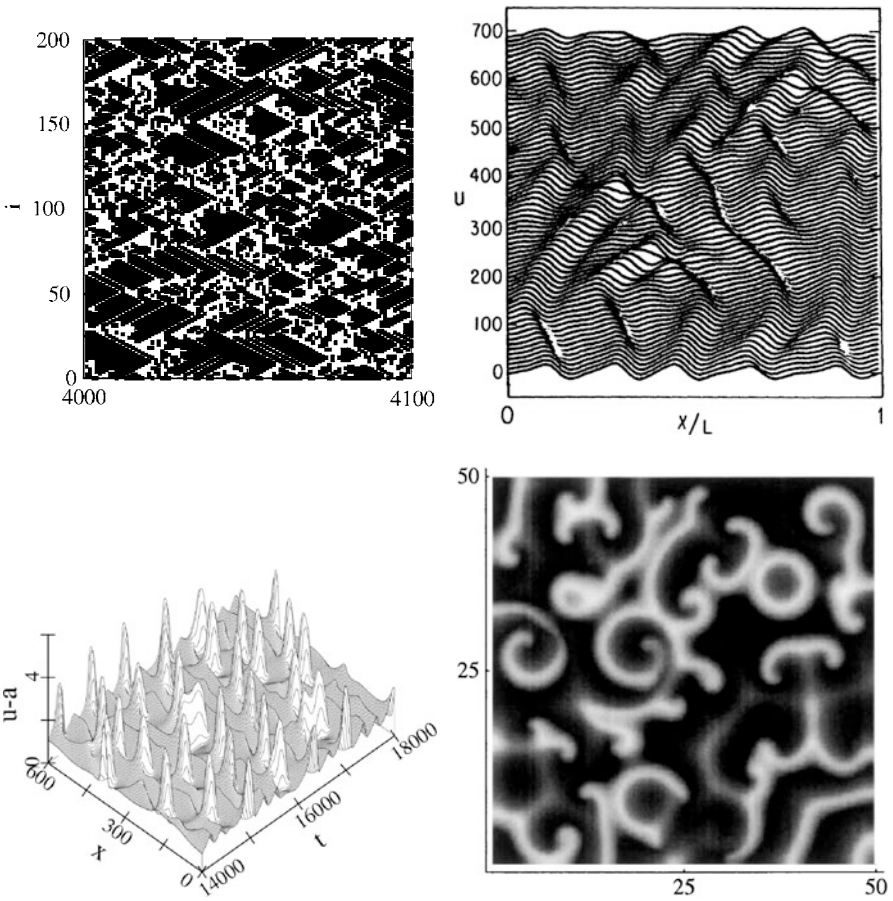

Fig. 9.1 *Upper left*: space-time diagram of a CML. Black (*white*) dots correspond to sites in a laminar (chaotic) regime. Horizontal (vertical) axis represents time (space) [797] (with kind permission from Elsevier Science). *Upper right*: space-time diagram of a solution of the KS equation (9.2). The distribution of the field variable $u(x)$ is plotted at an instant of time [715] (copyright 1986, the American Physical Society). *Lower left*: space-time diagram of an RD problem in one spatial dimension. The third axis represents the difference between the two concentrations [812] (with kind permission from the Institute of Physics). *Lower right*: instantaneous spatial pattern of an excitable medium in two dimensions. *Shading* corresponds to the concentration of one substance. The pattern is similar to that from the cGL equation [741] (copyright 1998, the American Physical Society)

and $\psi(\mathbf{r})$ respectively. In RD problems and fluid dynamics, two functions define the phase space: the set of all possible concentrations $a(\mathbf{r})$ and $b(\mathbf{r})$ for the former and the set of all possible velocity and pressure fields $\mathbf{v}(\mathbf{r})$ and $p(\mathbf{r})$ for the latter, where the forms of the functions are determined by the boundary conditions. For example, for a fluid system described by the NS equation, all velocity fields vanish on walls at rest but take on the values of the velocities of moving walls.

A given spatial distribution of the field variable represents a point of the phase space. Any of them can be a possible initial condition. The time evolution of the system corresponds to a motion among different phase-space points, and traces out a continuous curve emanating from the point representing the initial state. The time evolution is unique, and the phase-space description is thus complete.

A convenient way of representing an infinite-dimensional phase space is to expand the field variable(s) in terms of a complete set of orthonormal basis functions. The expansion coefficients a_i, $i = 1, \ldots$, can also be considered phase-space variables. This expansion can be truncated at some index N if variables a_i with $i = N+1, N+2, \ldots$ are negligible with respect to global dynamics. Thus, even systems described by PDEs can be represented as high-dimensional systems with a finite number of degrees of freedom. In a finite-dimensional phase space, stationary solutions correspond to fixed points of the phase space. Stable stationary solutions are thus fixed-point attractors. Homogeneous periodic solutions or waves correspond to limit cycles. Complicated chaotic solutions can be associated with chaotic attractors or chaotic saddles. The phenomenon of long transients is naturally related to situations in which the chaotic set is a saddle, and in addition, this saddle is rather dense (although not entirely space-filling) in the phase space.

9.1.3 Spatiotemporal Intermittency

There is a large literature on the phenomenon of spatiotemporal intermittency (STI) [120, 121, 375, 376, 378, 379, 404]. Here we briefly review this phenomenon, in order to distinguish it from concepts appearing later in this chapter. The concept of STI applies to spatiotemporal systems in which any space-time point can be classified as either *laminar* or *turbulent*. By "laminar" we mean a regular pattern (whose temporal dynamics might be both regular and chaotic), while "turbulent" regions have no apparent regularity either in space or in time. Spatiotemporal intermittency implies that there are intervals in both space and time in which one of the phases dominates. Domains of a given type of behavior have well-defined boundaries. An example is provided by the upper left panel of Fig. 9.1. There were many experiments on STI (for recent examples, see [269, 478, 659]).

Spatiotemporal intermittency is not the only possible manifestation of spatiotemporal chaos, but it is certainly a typical one. It can be considered as state of transition between laminar and fully turbulent phases. This does not imply that STI must evolve to be more and more complicated. Spatiotemporal intermittency can very well provide an asymptotic state, a spatiotemporally chaotic attractor. The usual statistical measures of STI consider long-time averages of spatial characteristics, such as the distributions of the size of laminar regions and of the "turbulent" regions [120, 121]. In a spatiotemporally intermittent state both distributions are exponentially decaying. The decay constants are related to the sizes of the average laminar or turbulent phases. A difference between the characters of these distributions typically

appears at the onset of STI. Here the distribution of the laminar domains follows a power law, indicating the lack of any characteristic sizes. The onset is, therefore, similar to a phase transition.

We wish to emphasize that STI can also characterize long transients [376, 619, 831]. In fact, many transients in spatiotemporal systems are of this type. We shall see that the lifetime can be sufficiently long to make statistical properties stationary (similar to, e.g., the statistics needed to determine the average Lyapunov exponent on a chaotic saddle in low-dimensional systems).

9.2 Supertransients

9.2.1 Transient Chaos in Coupled Map Lattices

Perhaps the first indication of complex spatiotemporal patterns appearing as long-lived transients was found in the thermal convection experiments by Ahlers and Walden, as early as 1980 [9]. For a detailed investigation of these transients, however, CMLs have proven to be convenient model systems, initiated by the seminal paper of Crutchfield and Kaneko [146].

The CML (9.1) has been studied extensively for different types of map f. The initial conditions are most frequently taken as random numbers at each site. When the map is strictly contracting, the asymptotic behavior is always spatially regular and temporally periodic (often homogeneous and steady). The transients toward this state are, however, typically chaotic. For map f that produces transient chaos on its own with positive topological entropy but possesses periodic attractors, the asymptotic behavior can often be spatially regular and temporally periodic. The CML built on the map f with chaotic attractors generates permanent spatiotemporal chaos if the coupling is weak, but transient chaos leading to a simple attractor is common for intermediate and strong couplings [831]. These results are summarized in Table 9.1. An observation is that diffusive coupling can generate chaos even from nonchaotic maps, and it often converts permanent local chaos into global transients.

A question is how the average transient lifetime $\tau \approx 1/\kappa$ depends on the system size L. For weak coupling $\varepsilon < \varepsilon_0$, practically no size-dependence is found. For slightly stronger coupling, however, the lifetime increases rapidly with the

Table 9.1 Dynamics of the map f and of the corresponding CML

Map f	CML
Nonchaotic	Transiently chaotic [146, 228, 387, 487, 609, 610]
Transiently chaotic	Transiently chaotic [377]
Permanently chaotic	Transiently chaotic [465, 619, 831]
	Permanently chaotic [619, 831]

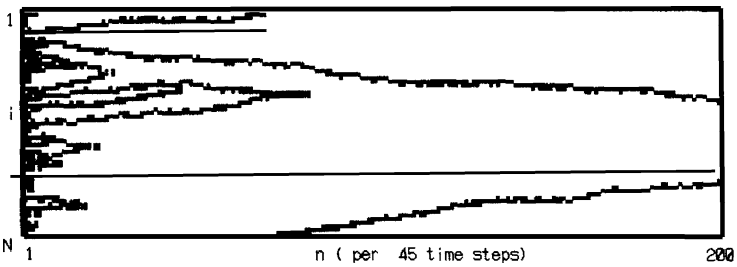

Fig. 9.2 Typical space-time pattern of type-I supertransients [377] (with kind permission from Elsevier Science)

system size. These are the *supertransients* [146]. There are two distinct types of supertransients. *Type-I supertransients* are characterized by a power-law scaling

$$\kappa(L) \sim L^{-\beta} \tag{9.7}$$

with a positive exponent β. *Type-II supertransients* are characterized by an exponential scaling:

$$\kappa(L) \sim \exp(-aL^{\gamma}), \tag{9.8}$$

where γ is a positive exponent and the coefficient a in general depends on the system parameters.

The patterns associated with the two types of supertransients are qualitatively different. For type-I supertransients, the basic features are defects whose density decreases gradually with time, as shown in Fig. 9.2. This can also be considered as a kind of aging process. Correspondingly, dynamical invariants such as the Lyapunov exponents and entropies also decrease with time.

Type-II supertransients are, in contrast, statistically steady over a long period of time, i.e., averages are time-independent in the chaotic state, and the transition to an attractor is rather abrupt, as exemplified by Fig. 9.3. If the maximum Lyapunov exponent is positive, a chaotic saddle is expected to exist in the high-dimensional phase space.

9.2.2 Origin of Supertransient Scaling

The different scaling rules can be traced back to the different patterns that are characteristic of the two classes of supertransients.

Type-I supertransients: The dominant process is that the defects, as indicated in Fig. 9.2, undergo a kind of random walk, and when they meet, they annihilate. For an anomalous random walk, the variance of the displacement scales with time as $t^{1/\beta}$, where β is a positive number ($\beta = 2$ corresponds to normal diffusion). Estimating

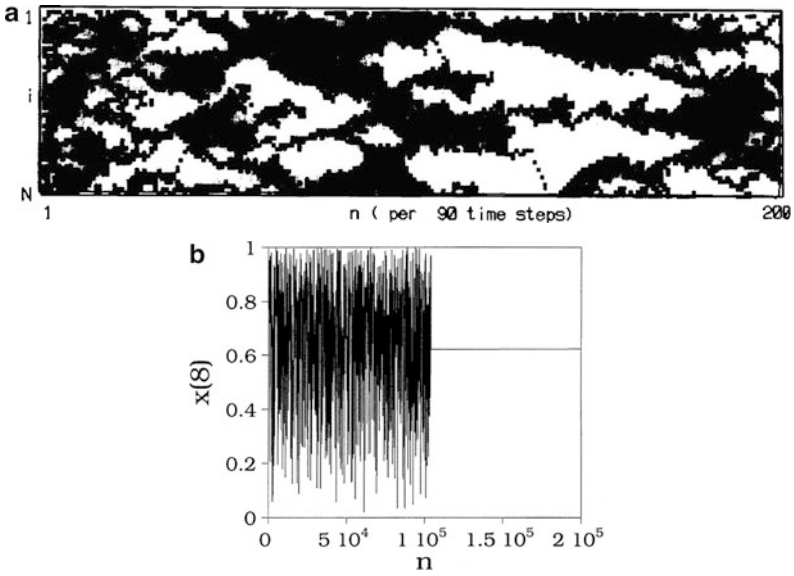

Fig. 9.3 (**a**) Typical space-time pattern of type-II supertransients. From [377] (with kind permission from Elsevier Science). (**b**) Time-dependence at a single site illustrating that the crossover to the nonchaotic behavior is abrupt [465] (copyright 1995, the American Physical Society)

the average lifetime τ as the time needed to reach a displacement variance of the order of the system size, we obtain $\tau \sim L^{\beta}$, which is equivalent to (9.7).

Type-II supertransients: Let $x^*(i)$ denote the coordinate corresponding to the regular spatiotemporal attractor at site i. A basin size r can be found that is much smaller than the system size in the following sense: if $|x_0(i) - x^*(i)| < r$ for *all* sites, the system reaches the attractor without chaotic excursions, but if the difference is larger than r, irregular transients appear. This basin size is a measure of the extension of the attractor's basin, restricted to a single dimension. The probability P that a randomly chosen initial condition at some of the sites falls within the basin size is proportional to this size: $P \sim r \ll 1$.

The following intuitive argument can be used to explain the scaling with the system size [228, 377, 619, 812]. In a spatially extended system there exists a correlation length ξ, within which neighboring sites move in a coherent manner. Conversely, only sites farther apart than ξ move independently. The system can thus be divided into L/ξ subunits that behave independently. For a random initial condition, the probability Π of falling into all the local basins is P raised to the power of the number of independent units, i.e., $\Pi \sim P^{L/\xi}$. Time needed to reach the hole is the phase space of the basin size is proportional to $1/\Pi$, and thus the average lifetime is estimated as

$$\tau(L) \sim \Pi^{-1} \sim P^{-L/\xi} \sim r^{-L/\xi} \sim \mathrm{e}^{aL}, \tag{9.9}$$

where $a = (\ln 1/r)/\xi$ is a positive constant. Here we have assumed that the basin size is independent of the system size. A strong dependence of r on L can modify the result. If, for example, $r = r(L) \sim \exp(-L^{\gamma-1})$, we have $\tau(L) \sim \exp(L^{\gamma}/\xi)$ (cf. (9.8)). Numerical computations often support, however, a linear length-dependence in the exponent, indicating a weak dependence of the basin size on L.

Finally, we note that the problem of supertransients is effectively the high-dimensional analogue of chaos in well-stirred chemical reactions in *closed* containers. In the absence of any material flux, the final state can be only in thermal equilibrium governed by a fixed-point attractor. With initial conditions far away from the thermal equilibrium, one brings the system into a regime whereby long chaotic transients can arise, as pointed out by Scott, Showalter, and coworkers (see Fig. 1.15). The novel feature in spatiotemporal systems is that nearly all initial conditions are far away from the attractor, since the probability of falling into the basin of attraction is extremely small.

9.2.3 *Supertransients with Exponentially Long Lifetimes in Other Systems*

It is remarkable that supertransients, mainly of type II, appear in a large number of systems other than CMLs. Typically, the lifetime scales with the system size as

$$\kappa(L) \sim \exp(-aL). \tag{9.10}$$

Evidence for this behavior has been found in a number of systems, as follows.

Kuramoto–Shivashinsky equation. The investigations of Shraiman [715] and of Hyman, Nicolaenko, and Zalesky [348] on phase turbulence in the one-dimensional KS equation (9.2) provided the first examples of supertransients in a PDE system, discovered earlier than those in CMLs. The upper right panel of Fig. 9.1 shows a typical transient pattern.

Complex Ginzburg–Landau equation. After a detailed numerical analysis of long-lasting spatiotemporal turbulence in the two-dimensional cGL equation by Bohr and coworkers [85, 86, 344], Braun and Feudel [98] and Houghton and coworkers [340] provided numerical evidence for an exponential scaling of the average transient lifetime with the system size.

Reaction–diffusion systems. The first example of type-II supertransients in RD systems of the type (9.5) in one spatial dimension was found by Wacker, Bose, and Schöll [812]. A typical concentration distribution in the transient phase can be seen in the lower left panel of Fig. 9.1. A decomposition of patterns during the transients into eigenmodes indicates that there exist no preferred modes [516–518]. Transient patterns are thus shown to be uncorrelated, a feature underlying the argument leading to type-II supertransient scaling. The study of RD systems was extended by Wackerbauer, Showalter, and coworkers [813–815, 842].

Two-dimensional excitable medium. The model investigated by Strain and Greenside [741] differs slightly in structure from (9.5), but exhibits similar dynamical behavior, although with different types of patterns in two dimensions (lower right panel of Fig. 9.1). This is the first PDE model in which the fractal properties of a high-dimensional chaotic saddle were investigated (Sect. 9.5).

Complex networks. An observation of Zumdieck, Timme, Geisel, and Wolf [858] was that in a randomly diluted set of coupled oscillators, the transients toward a limit-cycle attractor are chaotic and exhibit the scaling (9.10), with the number of oscillators replacing the length L. The average lifetime of the transients depends also on the network connectivity, and reaches a maximum at as intermediate level of dilution. Irregular and exponentially long transients were also observed in different neural network models [178,428,855,856]. Supertransients with exponentially long lifetimes were also observed in social networks [51, 52].

Turbulent shear flow. The Theoretical work of Eckhardt and coworkers (see, e.g., [229,231]) based on the Navier–Stokes equation (9.6) predicted the long-lived transient nature of turbulence in pipes. Recent experiments by Hof et al. [334, 336] provided evidence for a type-II (or even stronger) supertransient scaling, where the quantity in (9.10) is replaced by the Reynolds number (for more detail see Sect. 9.6).

9.2.4 Stable Chaos

A peculiar feature of type-II supertransients is that the maximum Lyapunov exponent is in certain cases negative even *during the transients*, although the transient patterns are as irregular as otherwise. This phenomenon has been called stable chaos [609,610] and provides an example whereby linear stability can coexist with nonlinear instability in the transient phase. Following the definition of Politi and coworkers [856], stable chaos means transients that (1) have a negative or zero maximum Lyapunov exponent and (2) appear stationary for long times, the average of which scales with the system size exponentially. The phenomenon is robust also in the sense that it can be present in finite regions of the parameter space [609].

Stable chaos was first found in CMLs for which the local map f is piecewise linear, is discontinuous at certain points, and possesses a simple periodic attractor. The map f can be contracting [146,228,857] or can have expanding pieces [62,148,609]. The transients are in any case random, illustrated by an exponential decay in both the temporal and the spatial correlations. These features are not due to the discontinuity in f, because a continuous variant of the map, in which the discontinuity is replaced by a steep continuous line, has been shown to exhibit the same behavior [228,609]. The supertransients as such maps are nonchaotic in the sense of sensitive dependence on initial conditions, but are chaotic in the sense of positive topological entropy.

The irregular behavior of stable chaos cannot be related to a local production of information, due to the lack of a positive Lyapunov exponent. Investigations [118, 264, 610, 784] led to the conclusion that the irregularity associated with stable

chaos is produced by transport, i.e., by the nonlinear propagation of finite disturbances. The so-called *damage spreading* analysis [833] can therefore be used to understand the phenomenon of stable chaos. In particular, one is interested in the effect produced by finite localized perturbations. Indeed, in systems exhibiting stable chaos [118, 264, 610, 784], initially perturbed regions in space spread with a *constant* front velocity v. Disturbances can thus travel through the system without damping. It is this velocity that plays in some sense the role of a positive Lyapunov exponent.

Stable chaos often appears in a certain range of a control parameter, e.g., the coupling constant ε in (9.1). Outside this range, there are no long transients and the system rapidly reaches a synchronized, periodic state, in which the front velocity v is zero. The transition is, however, not a single point in the parameter space. It occurs in an extended interval [118], where ordered and chaotic dynamics characterized by $v = 0$ and $v \neq 0$, respectively, alternate in a quite irregular manner.

Stable chaos is not restricted to CMLs. Bonaccini and Politi [91] considered coupled nonchaotic oscillators in continuous time. The oscillators are subject to a synchronous periodic forcing over a period T, which is suddenly changed to an unforced state of length T', and this mechanism is repeated periodically. For sufficiently rare active driving where T/T' small, the largest Lyapunov exponent of the coupled-driven system is negative, and the system exhibits properties of stable chaos. The diluted neural network model [856] mentioned in Sect. 9.2.3 was shown to follow the scaling (9.10) in a certain range of parameters, where all Lyapunov exponents are negative during the transients.

In all the continuous-time examples, the dynamics is associated with the presence of discontinuities, or with being close to such singularities. In the oscillator model there is a sudden change in the driving mechanism, and in the neural-network model the discontinuity is connected with changes in the spike ordering. Thus one can conclude [172, 856] that discontinuities or rapid changes in the dynamical equations are a necessary condition for the onset of stable chaos. A detailed review of stable chaos can be found in [611], which also presents an additional realistic system with stable chaos: a diatomic gas of hard-point particles.

9.3 Effect of Noise and Nonlocal Coupling on Supertransients

Numerical results on the effect of noise on supertransients in spatially extended dynamical systems were obtained in [433] for a CML system. The diffusive coupling constant ε in (9.1) was replaced by a random variable $\varepsilon \to \varepsilon + \sigma\xi_n$, where ξ_n is a random number taken at time instant n, and σ represents the noise intensity. This choice of noise is homogeneous over the full system, i.e., ξ_n does not depend on the site index i. The average lifetime was found to depend little on the noise intensity σ in the weak-noise regime, suggesting that supertransients are robust [850].

A more recent investigation of Wackerbauer and Kobayashi [814] considered the effect of spatially inhomogeneous noise as well. They studied an RD system (9.5)

in one spatial dimension with periodic boundary condition. The continuous space dependencies in the concentrations $a(x,t)$ and $b(x,t)$ are approximated by a discrete set $[a^{(i)}(t), b^{(i)}(t)]$ of variables for $N \gg 1$ sites ($i = 1, \ldots, N$). Correspondingly, the diffusive coupling term is also discretized. This chain of variables can be considered to be arranged around a circle. Additive noise $\sigma\xi^{(i)}(t)$ is included in the chemical kinetic equation governing the concentration $b^{(i)}$. The chain is divided into k blocks such that N/k neighboring sites are subject to the same realization of noise. The noise terms acting on neighboring blocks are chosen to be independent. Any value $k > 1$ corresponds to a spatially inhomogeneous noise – the more inhomogeneous, the larger the value of k. The results show that spatially inhomogeneous weak noise tends to decrease the escape rate of supertransients up to a certain strength at which a minimum of the escape rate is reached, as shown in Fig. 9.4. The effect intensifies with the degree of the inhomogeneity parameter k. The scenario is similar to what occurs in a class of low-dimensional systems (Fig. 4.2). Qualitatively, weak inhomogeneous noise makes the system more random and reduces the chance of finding the small basin of the attractor. In this model, homogeneous noise ($k = 1$) has a destructive effect on the transients: it leads to a monotonic increase in the escape rate for increasing noise strength. However, type-II supertransient scaling remains valid in that the lifetime increases exponentially with the size even in the presence of noise.

In search of a method to control the length of supertransients, an approach is to investigate the effect of nonlocal coupling in the noise-free problem. Yonker and Wackerbauer [842] studied the consequence of adding a few nonlocal connections (shortcuts). At sites coupled not only to the nearest neighbors but to a third, more distant, site, they modified the discrete Laplacian so that all three sites are included in a way that ensures the same perturbation, the same as in the locally coupled model. The length s of the shortcuts is a basic parameter, which is defined as the minimal number of sites between the two end sites of the shortcut divided by the number N of sites in the ring. The longest shortcut connecting two opposite sites along the circle corresponds to length $s = 1/2$. For a single shortcut of small length,

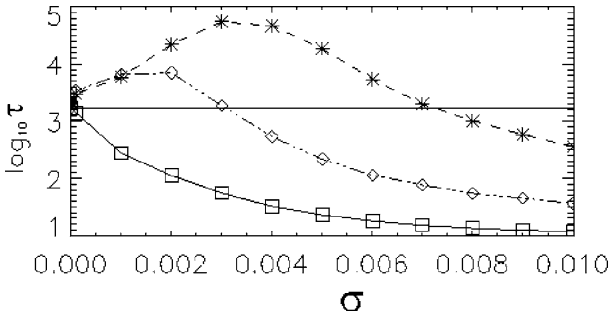

Fig. 9.4 Dependence of the average lifetime τ on the noise intensity σ in an RD system. The degree of spatial noise inhomogeneity k decreases from $k = 20$ (*stars*) to $k = 4$ (*diamonds*) to spatially homogeneous noise $k = 1$ (*squares*) [814] (copyright 2007, the American Physical Society)

the average lifetime increases, reaches a maximum at about $s = 0.05$, then decreases, finally leading to a reduced lifetime compared to that in the locally coupled system. The overall dependence is similar to that of the upper curves in Fig. 9.4. In any case, the type-II supertransient scaling remains valid for any s with a slightly s-dependent prefactor $a(s)$ in (9.10).

Adding more shortcuts can have a drastic effect on the transients. For example, two can have the local effect of stabilizing spatiotemporal chaos for arbitrarily long times, effectively preventing its collapse. Whether this can actually happen depends on the locations of the shortcuts and the initial conditions. For example, in a large ensemble of cases with randomly chosen shortcut locations, the probability for spatiotemporal chaos to be permanent is about 70%. Three shortcuts can increase the likelihood of permanent chaos even more. A further increase in the number of shortcuts, however, seems to weaken the effect, and the likelihood of transient chaos increases again.

Control of spatiotemporal transients via nonlinear feedback was suggested in [619], where it was demonstrated for a CML system that proper control can shorten the lifetime of the transients by several orders of magnitude. These developments illustrate that adding weak noise, or taking over methods from the physics of networks, has the potential to provide some effective ways to harness transient chaos in spatially extended systems.

9.4 Crises in Spatiotemporal Dynamical Systems

9.4.1 Boundary Crises: Supertransients Preceding Asymptotic Spatiotemporal Chaos

When there is an asymptotic spatiotemporal chaotic attractor, or asymptotic "turbulence," long chaotic transients typically occur in a parameter range preceding the permanently chaotic regime. Suppose the latter is in the parameter range $p > p_1$. Chaotic transients are then present for $p < p_1$. Intuitively, their average length should increase on approaching the critical value p_1. For supertransients, one expects a power-law divergence in the exponent of the average lifetime, i.e., a decay of the escape rate as

$$\kappa(p, L) \sim \exp\left[-c(L)(p_1 - p)^{-\delta}\right], \tag{9.11}$$

where $\delta > 0$ and the coefficient $c > 0$ depends on the system size L. Combining this with the size dependence of (9.8) or (9.10), we see that the coefficient a changes with the parameter p as

$$a(p) \sim (p_1 - p)^{-\delta}. \tag{9.12}$$

A detailed investigation of the two-dimensional cGL equation (9.4) led to the conclusion [85, 86, 344] that permanent spatiotemporal chaos is present in a region of the parameter plane (α, β) (μ fixed). When approaching the boundary of this

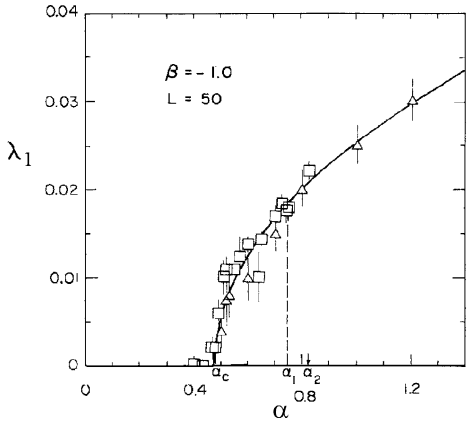

Fig. 9.5 For the cGL equation (9.4), the largest average Lyapunov exponent λ_1 of the chaotic sets as a function of the parameter α. Spatiotemporal chaos is permanent for $\alpha > \alpha_1$. For $\alpha_c < \alpha < \alpha_1$, only chaotic transients are present [86] (copyright 1990, the American Physical Society)

region from outside, the scaling relation (9.11) was found with exponent $\delta = 2$, which is similar to that for low-dimensional supertransient systems (cf. (8.60)), but here the exponent δ is larger than unity, and a size-dependence is also present.

When the largest average Lyapunov exponent λ_1 of the attractor is plotted as a function of the parameter $p \equiv \alpha$, it is positive in the range $\alpha > \alpha_1$. This curve can be merged smoothly with the curve of the Lyapunov exponent for the transient regime, as shown in Fig. 9.5, illustrating that the spatiotemporal chaotic saddle is converted at α_1 into a chaotic attractor. The critical parameter value α_1 can thus be viewed as a point of crisis in the cGL system. The Lyapunov exponent vanishes at some $\alpha < \alpha_c$, so the transients are not chaotic for $\alpha < \alpha_c$. For α slightly larger than α_c, the exponent scales as $\lambda_f(\alpha) \sim (\alpha - \alpha_c)^{1/2}$ [85, 86].

9.4.2 *Interior Crises in Spatially Coherent Chaotic Systems*

An investigation of different types of crisis phenomena in the KS equation was carried out by Chian, Rempel, and coworkers [126, 631, 632, 634]. These authors used the form (9.3) of the equation in which the length is fixed but the parameter ν contains the size of the original system. A parameter range was chosen for which the dynamics is chaotic in time but remains coherent in space. A Fourier decomposition of (9.3) with $N = 16$ modes appeared to be sufficient to illustrate the crisis phenomenon. In particular, in a parameter range of ν, a periodic window was found, as seen by plotting the long-time values of the sixth Fourier component a_6 as a function of ν. The window is bounded by an interior crisis and a saddle-node bifurcation at its two ends (Fig. 9.6a). Inside the window the attractor is a period-3 orbit or is localized in three narrow bands. In both cases it is surrounded by an extended chaotic saddle. The concept of basic components, introduced in Sect. 3.3 to characterize low-dimensional crises, thus becomes applicable to high-dimensional problems. This *surrounding chaotic saddle* (SCS) was determined by the PIM-triple method (Sect. 1.2.2.4), and its projection on the a_6 variable is also

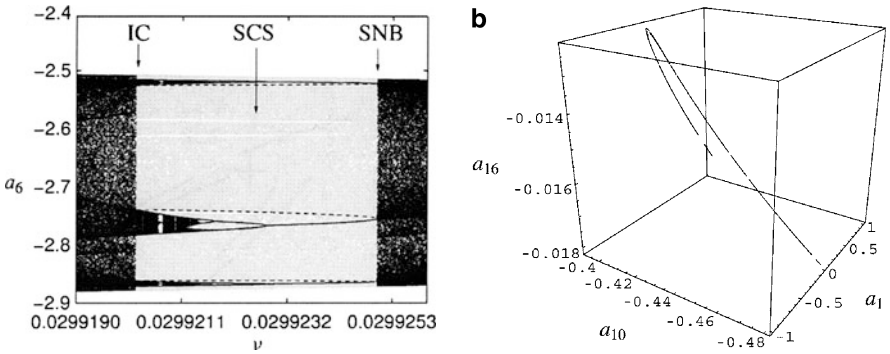

Fig. 9.6 Interior spatiotemporal crisis. (**a**) Bifurcation diagram of mode amplitude a_6 as a function of parameter ν in the KS equation (9.3). *Gray dots* indicate points on the surrounding chaotic saddle (SCS). IC and SNB denote interior crisis and saddle-node bifurcation, respectively. (**b**) A three-dimensional projection of the SCS for $\nu = 0.029925$ [631] (with kind permission from Elsevier Science)

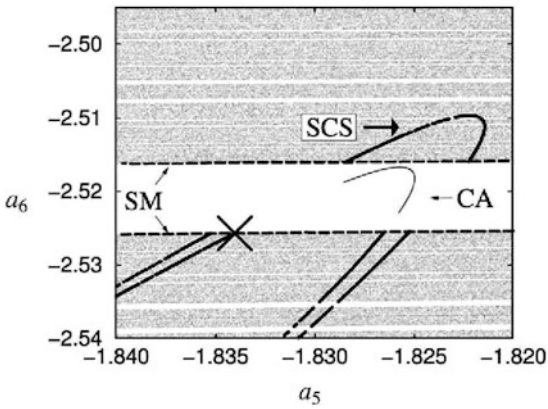

Fig. 9.7 Part of the phase space projected on the (a_5, a_6)-plane for $\nu = 0.0299211$, before interior crisis (IC). CA: chaotic attractor, SM: stable manifold of the mediating period orbit denoted by a *cross*. *Gray dots* mark the stable manifold of the SCS [631] (with kind permission from Elsevier Science)

shown in the bifurcation diagram. In the full phase space the chaotic saddle turns out to be extended but low-dimensional, as can be seen in a three-dimensional projection close to the saddle-node bifurcation, where no chaotic attractor exists. The saddle is practically a single line segment, but gaps are visible along this line (Fig. 9.6b).

In the middle of the window the attractor undergoes a period-doubling bifurcation, after which a small-size chaotic attractor (CA), the three-band attractor, appears. The surrounding chaotic saddle, SCS, coexists now with the chaotic attractor. In a projection onto the plane of two Fourier components, the stable manifold of the mediating periodic orbit separating the attractor from the saddle can be seen, as shown in Fig. 9.7. The saddle's stable manifold appears to be dense.

At the crisis, the small-size chaotic attractor collides with the mediating orbit or with its stable manifold, and thus with the chaotic saddle as well (Fig. 9.8a).

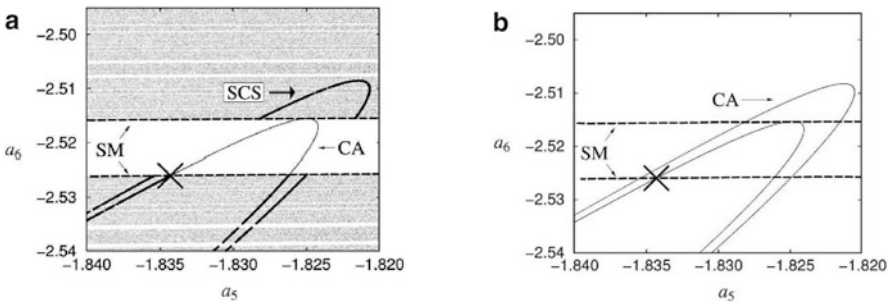

Fig. 9.8 Phase-space projection on the (a_5, a_6)-plane at IC, $\nu = 0.02992021$ (**a**), and slightly beyond crisis (**b**) [631] (with kind permission from Elsevier Science)

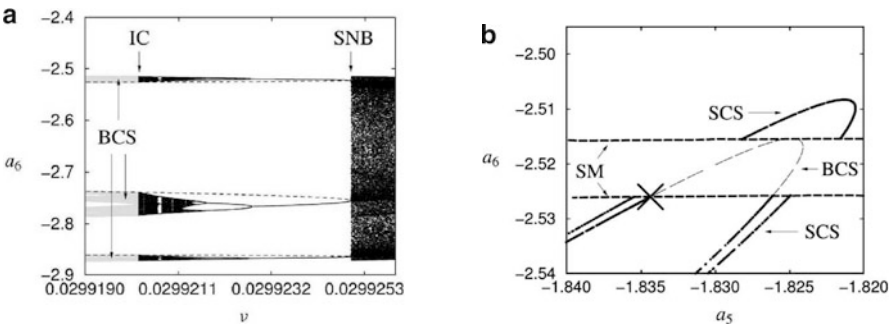

Fig. 9.9 (**a**) Bifurcation diagram as in Fig. 9.6 containing only the band chaotic attractor, which is converted into a band chaotic saddle (BCS, plotted in *gray*) beyond the interior crisis. (**b**) Chaotic saddles forming the backbone of the extended chaotic attractor projected on the (a_5, a_6)-plane at the postcrisis parameter value $\nu = 0.02992006$ [631] (with kind permission from Elsevier Science)

The large gaps present along the surrounding saddle just before the crisis become filled up by the newly generated orbits (see Sect. 3.4), and the extended chaotic attractor to appear contains the previous attractor, the saddle, and the filled-up gaps (Fig. 9.8b). After the crisis, points of the extended attractor that remain forever on the three bands occupied by the small attractor in the precrisis regime are connected to a saddle situated in this region, the *band chaotic saddle* (BCS). This saddle can be represented both on the bifurcation diagram (Fig. 9.9a) and on a projection of the plane of two variables (Fig. 9.9b). Similarly, points never leaving the region of the former surrounding chaotic saddle form a postcrisis chaotic saddle (SCS) that can be considered the continuation of the precrisis SCS. These two saddles are the main building blocks of the extended chaotic attractor arising from the interior crisis. The situation is thus similar to that for low-dimensional maps (Chap. 3).

9.4.3 *Crises Leading to Fully Developed Spatiotemporal Chaos*

In another series of papers, Rempel, Chian, and coworkers [633, 638] aimed to understand crises underlying spatiotemporal inhomogeneities [320]. For this purpose they used a one-dimensional PDE model of regularized long waves for a field $\phi(x,t)$ driven sinusoidally both in space and time. With all other parameters fixed, the main control parameter is the driving amplitude f. A Fourier decomposition of $\phi(x,t)$ into $N = 32$ spatial modes was used. As f is changed, the dynamics exhibit three qualitatively different types of behavior. For the lowest value of f the pattern is regular in space and quasiperiodic in time (Fig. 9.10a). For higher values of f, spatial regularity remains but the pattern becomes temporally chaotic (Fig. 9.10b), as indicated by the appearance of a positive Lyapunov exponent. The corresponding attractor is called a temporally chaotic attractor (TCA). A further increase in f leads to the appearance of fully developed spatiotemporal chaos (Fig. 9.10c). This occurs suddenly and is accompanied by an increase in the maximum Lyapunov exponent to a much larger value. The new attractor is a spatiotemporally chaotic attractor (STCA) that possesses a larger dimension value than the previous one (the TCA).

To follow these changes in the phase space, Rempel and Chian projected the invariant sets on the plane defined by the real parts of the second and the third Fourier modes, after taking an appropriate Poincaré map. The quasiperiodic torus attractor appears to be associated with a few closed curves (Fig. 9.11a). The authors

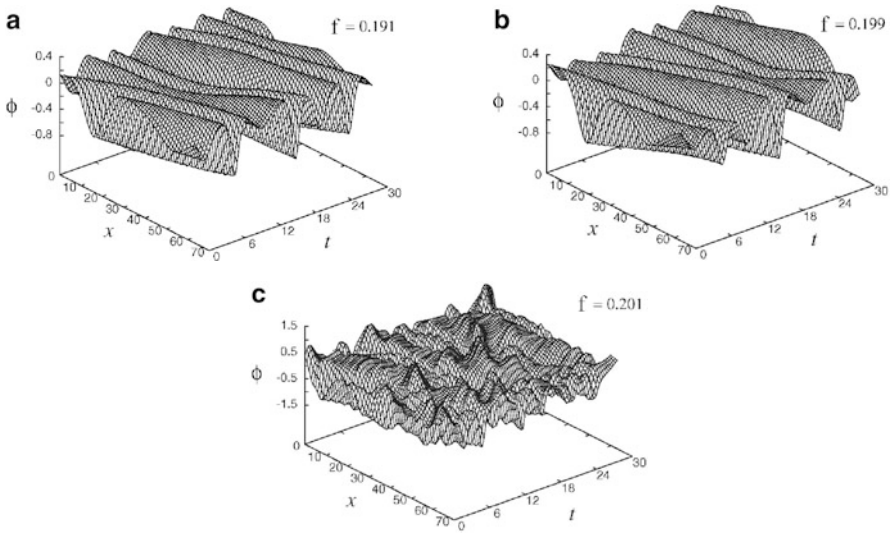

Fig. 9.10 Spatiotemporal patterns of the field ϕ for different values of the driving amplitude f: (**a**) spatially regular, temporally quasiperiodic; (**b**) spatially regular, temporally chaotic; and (**c**) spatially irregular, temporally chaotic [633] (copyright 2007, the American Physical Society)

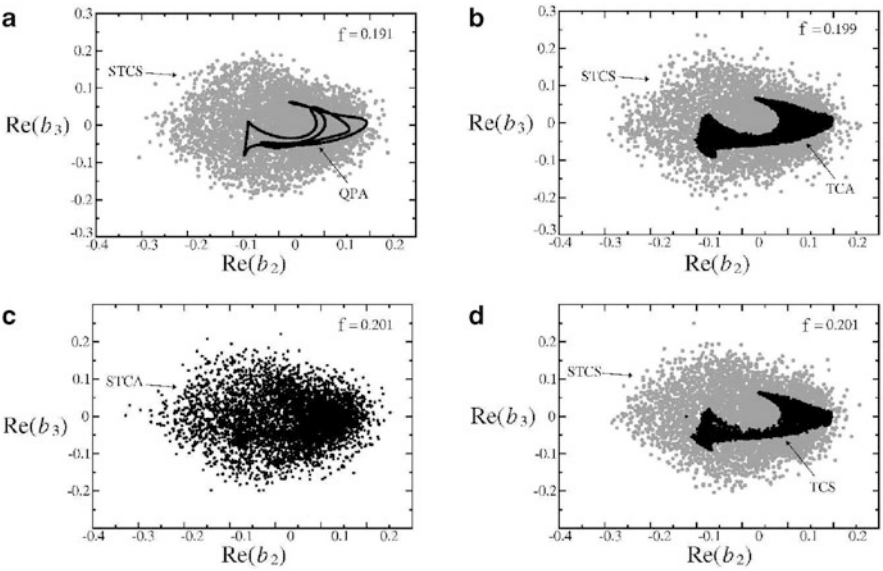

Fig. 9.11 Phase-space projection of various invariant sets on the plane of two modes. (**a**) A quasiperiodic attractor (QPA, *black*) and a spatiotemporally chaotic saddle (STCS, *gray dots*), (**b**) Temporally chaotic attractor (TCA), (**c**) a spatiotemporally chaotic attractor (STCA) after crisis, which occupies the regions where the former STCS and TCA reside, and (**d**) decomposition of STCA into a postcrisis STCS and a temporally chaotic saddle TCS after the crisis [633] (copyright 2007, the American Physical Society)

pointed out that already here an extended chaotic saddle exists surrounding the attractor. The corresponding transients carry irregular spatiotemporal patterns, and therefore the saddle is called the spatiotemporally chaotic saddle (STCS). When the spatially regular dynamics becomes chaotic, the torus attractor breaks, but the new temporally chaotic attractor (TCA) remains localized around the former torus (Fig. 9.11b). The TCA is area-filling in the projection, but is of small size. The surrounding saddle, STCS, does not change appreciably. When permanent spatiotemporal chaos occurs, the chaotic attractor suddenly broadens and becomes a spatiotemporally chaotic attractor (STCA); Fig. 9.11c. It is remarkable that the extension of the STCA is practically the same as that of the spatiotemporal saddle (STCS) earlier. At this crisis the temporally chaotic attractor collides with the surrounding saddle, and the latter becomes embedded in the new attractor. In this postcrisis regime, Rempel and Chian were also able to identify a chaotic saddle in the region occupied by the temporal attractor earlier. This saddle is called the temporally chaotic saddle (TCS); Fig. 9.11d. In the projection, it fills a slightly smaller area than the TCA.

If a trajectory on the extended attractor comes to the vicinity of the TCS, a regular pattern appears in the space, which changes chaotically in time. After some time, the trajectory deviates from this saddle, and comes close to the chaotic saddle that exists outside the TCS, a postcrisis STCS that governs the spatiotemporally chaotic

dynamics. After escaping from the STCS, the trajectory returns to the vicinity of the TCS and the pattern becomes regular again, etc. The average lifetime of the spatially regular phases can, in principle, be estimated as the average lifetime on the TCS. The full process is intermittent [131], and the situation is the high-dimensional analogue of crisis-induced intermittency discussed in Sect. 3.3. A similar phenomenon was observed in the damped KS equation [635].

The spatiotemporal intermittency (STI) mentioned in Sect. 9.1.3 is not the kind of intermittency treated here, since regular and irregular phases extend in STI over finite regions of the real space only. It may be useful to study spatiotemporal intermittency in terms of the underlying chaotic saddles. At present, little is known about the scaling with system size of the lifetimes associated with the intermittent dynamics discussed here.

9.5 Fractal Properties of Supertransients

9.5.1 Dimensions

Supertransients have specific fractal properties, as emphasized in [462–465]. It has been observed that chaotic saddles underlying long transients typically have a stable manifold whose dimension is close to that of the phase space. The basin of attraction of the regular asymptotic attractor can be determined on a plane of initial conditions of just a few variables (Fig. 9.12a). In a long observation time only a few points converge to the attractor; the others remain away from it. These points represent initial conditions that stay close to the chaotic saddle's stable manifold. Alternatively, in a

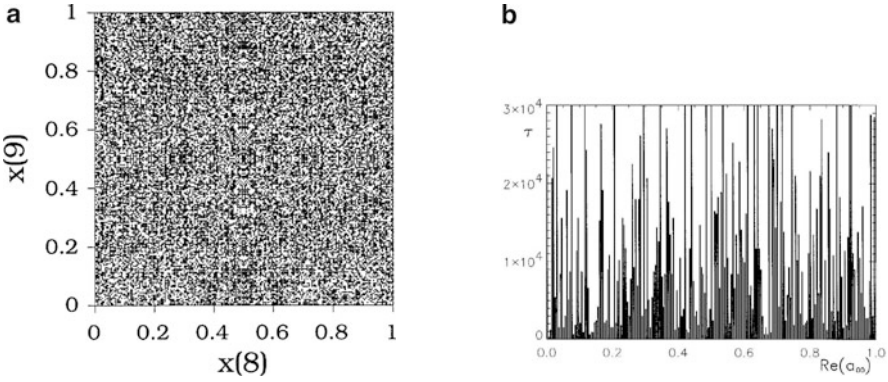

Fig. 9.12 (**a**) Stable manifold of a chaotic saddle (*black dots*) in the plane of two variables of a CML described by (9.1) [465] (copyright 1995, the American Physical Society). (**b**) Transient lifetime as a function of the initial condition taken from a one-dimensional line in the phase space of the cGL equation in its supertransient state [98] (copyright 1996, the American Physical Society). The dimension of the set of points with long lifetimes is denoted by d_s

plot of the lifetime function, the lifetimes needed to reach the attractor as a function of a single initial coordinate also appear to be dense (Fig. 9.12b). It is useful to introduce, as in scattering problems (Sect. 6.2), the box-counting dimension d_s as the dimension of the set of points where the lifetime is formally infinite along such a segment. Since infinite lifetime values belong to the stable manifold of the saddle, this d_s is the dimension of the intersection of a line with the stable manifold of the saddle.

As a quantitative measure of the fractality, the uncertainty exponent (Sect. 5.3) can be determined. The numerical value of α was found to be as small as 10^{-3} (cf. Fig. 9.13), indicating that d_s is quite close to unity. It was also shown [462–464] that the largest Lyapunov exponent computed at fixed finite time is extremely sensitive to small changes in the parameters. Supertransients are thus characterized by riddled structures in the parameter space.

A simple formula for the partial dimension d_s was conjectured in [465]. In particular, escape occurs mostly along the direction of the largest positive Lyapunov exponent $\lambda_{\max}$. The system is therefore expected to behave effectively as a two-dimensional system with positive Lyapunov exponent $\lambda_{\max}$. Utilizing the Kantz–Grassberger relation (2.76), one obtains the following information dimension $d_{s,1}$ of the set of singularities:

$$d_{s,1}(L) = 1 - \frac{\kappa(L)}{\lambda_{\max}}. \tag{9.13}$$

Taking into account that the dimension of a set resulting from the intersection of two sets follows from the rule according to which the codimensions are additive, (8.52), one finds for an N-dimensional map that the information dimension $D_{s,1}$ of the stable manifold is given by

$$D_{s,1}(L) = N + d_s - 1 = N - \frac{\kappa(L)}{\lambda_{\max}}. \tag{9.14}$$

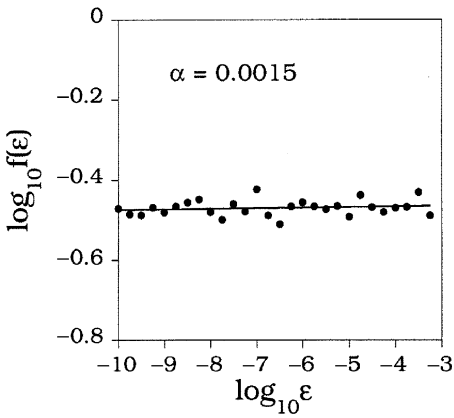

Fig. 9.13 Plot of the fraction of uncertain initial conditions $f(\varepsilon)$ versus uncertainty ε. With the value of the uncertainty exponent α, the box-counting dimension d_s is $d_s = 0.9985$, a quantity that is hardly distinguishable from unity [465] (copyright 1995, the American Physical Society)

We see that since κ is small, the dimension of the stable manifold is close, for type-II supertransients exponentially close, to the dimension of the phase space.

Equation (9.14) in fact follows directly from the general dimension formulas in Sect. 8.2.2. In particular, consider an $(N \gg 1)$-dimensional map with a small escape rate. When κ is nearly zero, the only possibility for the left-hand side of (8.23) to be larger than K_1 is that all the positive Lyapunov exponents appear on the right-hand side, i.e., $J+1=U$. The numerator in the ratio in (8.24) then contains $\lambda_U^+ - \kappa = \lambda_{\max} - \kappa$. Since $S+J = S+U-1 = N-1$, we recover (9.14).

The dimension formula (8.21) for the unstable manifold can also be applied. For spatiotemporal systems with small escape rate, observe first that the condition (8.20) requires that the sum of all Lyapunov exponents (with signs taken into account) up to index I be greater than κ, but up to index $I+1$ be smaller than κ. For near-zero values of κ, the sums should practically be positive and negative, respectively. This is the condition in the Kaplan–Yorke formula (see (8.21) with $\kappa = 0$)

$$D_1 = U + I + \frac{\lambda_1^+ + \cdots + \lambda_U^+ - (\lambda_1^- + \cdots + \lambda_I^-)}{\lambda_{I+1}^-} \tag{9.15}$$

for chaotic attractors. One can then imagine a chaotic attractor with the same Lyapunov exponent spectrum as the saddle, and denote its information dimension by $D_{\mathrm{attr},1}$. Given a discrete set of Lyapunov exponents, a small κ does not change the value of I, and we can write

$$D_{\mathrm{u},1}(L) = D_{\mathrm{attr},1} - \frac{\kappa(L)}{\lambda_{I+1}^-}. \tag{9.16}$$

For the saddle's dimension we then obtain, from (9.14),

$$D_1(L) = D_{\mathrm{attr},1} - \kappa(L)\left(\frac{1}{\lambda_{\max}} + \frac{1}{\lambda_{I+1}^-}\right) = D_{\mathrm{u},1}(L) - \frac{\kappa(L)}{\lambda_{\max}}. \tag{9.17}$$

Equations (9.14), (9.16), and (9.17) illustrate that a supertransient chaotic saddle is a *quasiattractor* in the sense that its dimension is close to that of an attractor (with almost identical Lyapunov spectrum), its stable manifold is nearly space-filling (close to forming a basin of attraction), and its unstable manifold has nearly the same dimension as the chaotic saddle (for an attractor, $D_{\mathrm{u},1}$ and D_1 coincide). These observations indicate that the dimension of supertransient chaotic saddles can be approximated by the Kaplan–Yorke formula, and explain why statistical averages are so well defined on supertransient chaotic saddles. The validity of relations (9.14) and (9.16) was recently illustrated for various high-dimensional reaction–diffusion systems [734].

It is worth mentioning that although the stable manifold is nearly space-filling, the unstable manifold's dimension can take on any value. It is the number U of positive Lyapunov exponents and the index I that essentially determine the value of $D_{\mathrm{u},1}$. In principle, it can assume a small value even in a high-dimensional phase space.

9.5.2 Dimension Densities

In high-dimensional systems it is useful to define dimension densities [85,487,831], i.e., quantities expressing the dimension falling on a single degree of freedom. For supertransients, the dimension density $\delta_s \equiv D_s/N$ of the stable manifold is close to unity. Little is known, however, about the dimension densities $\delta_u = D_{\mathrm{u},1}/N$ and $\delta = D_1/N$ of the unstable manifold and of the saddle, respectively. The question so far has been addressed in a few cases only. In particular, for a model of excitable media, Strain and Greenside [741], and for different RD systems, Stahlke and Wackerbauer [734], found the dimension density of the chaotic saddle to be of order a few percent. This is also consistent with the observation [516] that the number of positive Lyapunov exponents is small even in large systems (although the number increases with the system size).

An important dynamical property in high-dimensional systems is the existence of a Lyapunov density [85]. It implies that the set of the Lyapunov exponents $\lambda_j^{\pm}$, defined by (8.5), as a function of $x \equiv j/N$ converges for $N \to \infty$ to a well-defined function $\Lambda^{\pm}(x)$, as exemplified by Fig. 9.14. In such a case the number U of positive (or negative) Lyapunov exponents scales with the dimension of the phase space, and U/N converges to a constant. As a result, the metric entropy (8.9) can be written as

$$K = \int_0^{U/N} \Lambda^{+}(x)\mathrm{d}x - \kappa. \tag{9.18}$$

Similarly, the sums defining the indices J and I, (8.23) and (8.20), more precisely the ratios J/N and I/N, can also be expressed as integrals, which depend on the value of the escape rate. For small escape rates, however, the dependencies are weak, and

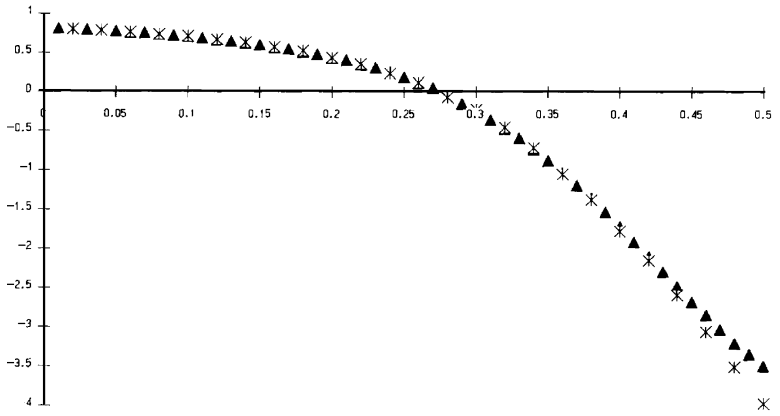

Fig. 9.14 Spectrum of Lyapunov exponents λ_j associated with chaotic transients for a CML of size $N = 50$ (*crosses*) and $N = 100$ (*triangles*), as a function of $x = j/N$. The convergence to a limiting Lyapunov density can be seen [487] (with kind permission from Elsevier Science)

we have $J/N = (U-1)/N \to U/N$. Since the fraction appearing in the general expression of $D_{s,1}$ and $D_{u,1}$ is always less than one, it does not contribute to the dimension density. Supertransients are thus characterized by the following dimension densities:

$$\delta_s = \frac{S+U}{N} = 1, \quad \delta = \delta_u = \frac{U+I}{N}. \tag{9.19}$$

It is worth defining the signed Lyapunov density $\Lambda(x)$, as shown in Fig. 9.14. Since, as stipulated by (8.5), $\Lambda(x) = \Lambda^+(U/N - x)$ for $0 \le x \le U/N$ and $\Lambda(x) = -\Lambda^-(x - U/N)$ for $1 \ge x \ge U/N$, the nontrivial dimension density $\delta_u = \delta$ also satisfies the equation

$$\int_0^{\delta_u} \Lambda(x)\,\mathrm{d}x = 0. \tag{9.20}$$

When considering the integral of the signed Lyapunov density between zero and some value x, the dimension density is the x value for which the integral vanishes. In fact, (9.20) is valid for spatiotemporal chaotic attractors as well [262]. We conclude that the picture based on the Lyapunov and dimension densities suppresses the role of the finite lifetime of chaos, and emphasizes the quasiattractor character of supertransients.

The problem of stable chaos (Sect. 9.2.4) deserves special attention. Although these systems appear to exhibit fractal features, dimension formulas (8.21) and (8.24) are not applicable. In fact, these relations are valid for generic chaotic saddles, but that is not the case here. There is a possibility for strange nonchaotic saddles to arise in analogy with strange nonchaotic attractors [241]. (For strange nonchaotic repellers of one-dimensional maps, see Sect. 2.4.) A strange nonchaotic spatiotemporal saddle might have a box-counting dimension that does not increase linearly with the system size, i.e., with a density $\delta_u = \delta = 0$.

9.6 Turbulence in Pipe Flows

9.6.1 Turbulence Lifetime

The transition to turbulence in pipe flows has long been a fascinating problem in fluid dynamics (for reviews, see [216, 217, 299]). Investigations of the phenomenon began in the second part of the nineteenth century with the milestone experiments of Reynolds in 1883. He pointed out that in a pipe of fixed length the flow changes from smooth (laminar) to irregular (turbulent) at sufficiently large flow velocities. A good dimensionless measure of the flow velocity is the Reynolds number $Re = UD/\nu$, with U and D chosen as the mean flow speed across the pipe and the diameter, respectively. When the flow velocity slowly increases in a given setting, the transition from laminar flow to turbulence occurs abruptly at a critical Reynolds number Re_c of order 2,000. Early experiments indicated, however, that under controlled conditions the laminar flow can be maintained up to Reynolds numbers much larger

than 2,000. It was recognized later that the roughness of the wall's surface plays an important role: the rougher the wall, the smaller the critical Reynolds number. More recent investigations have led to the observation that perturbations to the laminar flow such as those caused by surface roughness are needed to trigger turbulence, and the critical Reynolds number Re_c depends on the type and the strength of the perturbation. Thus the onset of turbulence is determined not only by the Reynolds number but also by the perturbation. To trigger turbulence, the flow has to be sufficiently fast and the perturbation has to be sufficiently strong. The required perturbation is, however, smaller for larger values of the Reynolds number. Therefore, in any experimental setting in which small perturbations cannot be avoided, turbulence will always appear at sufficiently large values of the Reynolds number.

The steady laminar solution, such as the parabola profile in a pipe of circular cross section, is linearly stable for *all* Reynolds numbers [299]. In dynamical-system terms, this implies the existence of a fixed-point attractor in the infinite-dimensional phase space, with a relatively small basin of attraction. In addition, there is no evidence for the existence of any stable state with simple spatial or temporal pattern, e.g., traveling waves, which would be the analogues of limit cycle attractors. The turbulent state can be considered a high-dimensional chaotic state associated with either a chaotic attractor or a chaotic saddle.

The first indication of the transient character of pipe turbulence appeared about 20 years ago [99, 299], based on investigations of the stability of the laminar profile. There has been increasing experimental evidence since then indicating that even if the turbulent state is established for not too large Reynolds numbers, this state can suddenly decay, without any apparent precursor, toward the laminar state. This implies that the chaotic sets for not too large values of the Reynolds number are nonattracting. Research has then been concentrated on the average lifetime τ of the chaotic saddle. The classical experiments suggest that the lifetime is rather large, for otherwise, the turbulence would not have appeared to be permanent to earlier investigators. The use of long pipes and efficient numerical methods have made more detailed investigations possible. Figure 1.23 shows the experimental findings of Peixinho and Mullin on the exponential decay in time. The value of the escape rate appears to be *independent* of the details of the initial perturbation, but depends on the Reynolds number only. The exponential decay sets in only after some time t_0 in any experimental run.

When plotting the actual lifetime as a function of the perturbation amplitude A to trigger the turbulence in numerical simulations, a more detailed picture can be obtained. A slight change in the amplitude can lead to drastically different lifetimes if the amplitude is above a threshold (Fig. 9.15). The irregular part of the lifetime distribution is fractal. Furthermore, the average Lyapunov exponent during the turbulent phase was shown to be strictly positive [231]. These features indicate that the high-dimensional saddle underlying the turbulence has all the characteristics of low-dimensional chaotic saddles and of transient chaos in many other spatiotemporal systems.

A basic question is the dependence of the turbulent escape rate on the Reynolds number. In the class of functions exhibiting a rapid decrease with the Reynolds

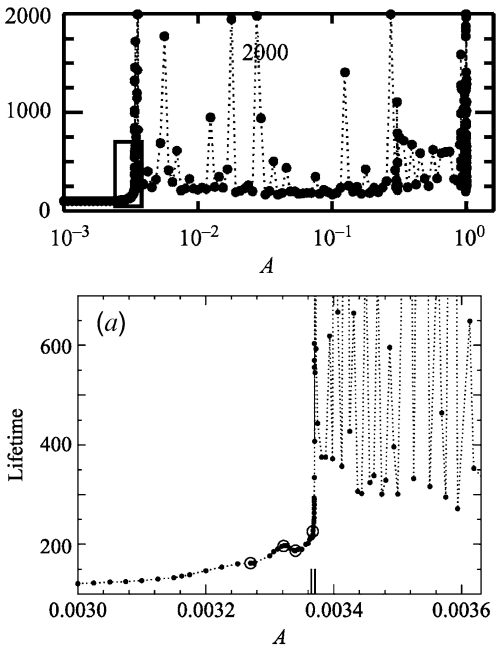

Fig. 9.15 Turbulence lifetime versus perturbation amplitude A in a pipe at Reynolds number $Re = 2{,}000$ obtained numerically. The *bottom panel* is a magnification of the box indicated in the *top panel*. At the edge of chaos, at the value marked by two *vertical bars*, the function turns from smooth to fractal-like, indicating that chaotic transients are triggered by sufficiently large amplitudes [231] (with kind permission from Cambridge University Press)

number, a choice is some functions that approach zero for a finite value of Re. This form can retain one aspect of the original picture, namely that beyond a threshold Reynolds number, permanent turbulence can be present. The laminar fixed-point attractor would then coexist with the chaotic attractor of the turbulence. Another choice is some monotonically decreasing functions of Re with nonzero values for any Re. Using a pipe of length 30 m, experiments by Hof, Westerweel, Schneider, and Eckhardt [336] provided a firm answer to the question. In a set of experiments covering more than two decades of lifetimes, they showed that the escape rate is nonzero up to large values of Re. This suggests that *turbulence remains a transient*, a feature also observed in superfluid turbulence [693] and magneto hydrodynamical turbulence [639]. By measuring time in units of D/U, the dimensionless escape rate was found in [160, 217, 336] to scale with Re as

$$\kappa(Re) = a\mathrm{e}^{-bRe} \tag{9.21}$$

with parameter b between 0.03 and 0.04 (see Fig. 9.16). According to this rule, any increase in the Reynolds number by 100 implies a multiplication of the escape rate by a factor of $1/33$. Thus, pipe turbulence is a kind of type-II supertransient (with system size replaced by the Reynolds number).

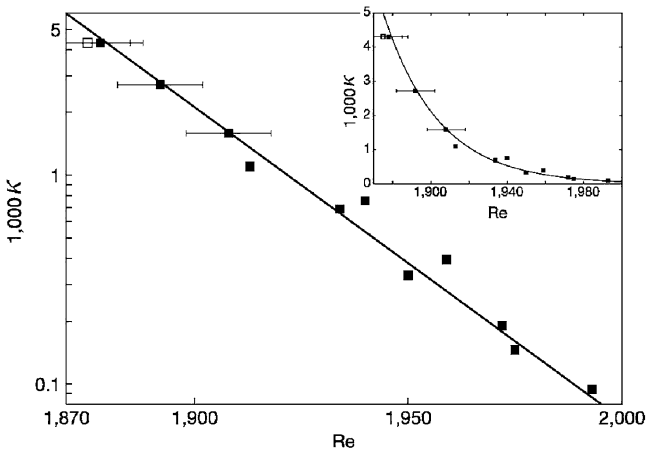

Fig. 9.16 Escape rate as a function of the Reynolds number in the experiment by Hof et al. The *straight-line* fit corresponds to formula (9.21). The *inset* shows the same data on a linear scale to illustrate that the escape rate is asymptotic to zero rather than crossing the horizontal axis at a finite value of Re [217] (with kind permission from Annual Reviews)

A recent experimental study by Hof, de Lozar, Kuik, and Westerweel [334] extended the range of turbulent lifetimes by six orders of magnitude by collecting data from four pipe setups with significantly reduced statistical errors. The extended data set (which contains, as a subset, the points of Fig. 9.16) suggests a superexponential scaling with the Reynolds number in the form of

$$\kappa(Re) = \exp\left[-\exp\left(c_1 Re + c_2\right)\right] \tag{9.22}$$

with $c_1 = 0.0057$, $c_2 = -8.7$. This fit is valid in the Reynolds-number range $(1670, 2040)$, where the dimensionless κ changes between 0.2 and 10^{-8}. Note that a further extension of these results is hardly possible, since due to the rapid increase in the lifetime, the measurement at $Re = 2,100$ would already require an estimated time of 46 years [334, 663].

Due to extended and improved numerical methods, the range of Reynolds numbers and sample sizes of experiments have become accessible in computer simulations. The results of [33] were in close quantitative agreement with the form of (9.22). Similar superexponential scaling of lifetimes was reported in a Taylor–Couette flow [95].

A possible theoretical explanation of the superexponential scaling was provided by Goldenfeld and coworkers [267]. The authors argued that the determining factor for the suppression of a puff is the probability that the largest velocity fluctuations fall below some threshold value. These large-amplitude events follow extremal statistics. From general results on such statistics the superexponential form of (9.22) can be derived.

9.6.2 Other Aspects of Hydrodynamical Supertransients

An interesting feature of the lifetime distribution versus perturbation amplitude, as shown in Fig. 9.15, is that slowly varying regions are interwoven with intervals of rapid change. In the smooth regions the transients are short and nonchaotic. The transition (indicated by two bars in Fig. 9.15) between the extended smooth region at small amplitudes and the region with fractal fluctuations is rather abrupt. This point on the border between laminar and chaotic regions is called the *edge of chaos* [691, 720], which separates initial conditions that decay directly to the laminar attractor and those that come close to the chaotic saddle first, i.e., exhibit turbulence. Trajectories starting from the edge of chaos move in a region intermediate between laminar and turbulent dynamics. The results of [409, 520, 691, 720, 803] suggest that the edge of chaos lies, for any Reynolds number, in the stable manifold of an invariant object, the edge state that resides in the phase space between the fixed point and the chaotic saddle. The stable manifold is thus a kind of basin boundary between the laminar and the turbulent dynamics. The latter, of course, cannot have a real basin of attraction, but only one that appears to be so in finite-time observations (the quasiattractor character discussed in Sect. 9.5). The dynamics restricted to the edge of chaos converges to a chaotic state, the edge state, and numerical simulations in pipe flows indicated that it corresponds indeed to an irregular wavy motion along the pipe, which is, however, less energetic than the turbulent dynamics itself [691]. This attractor is only a relative attractor, since it is unstable with respect to perturbations perpendicular to the edge of chaos.

Low-dimensional chaotic saddles contain an infinite number of unstable periodic orbits (Sect. 2.6.4). In an analogous way, the chaotic saddle underlying pipe turbulence is expected to contain coherent structures. Both in theory and experiments, they were shown to be regular traveling waves [229, 335], all *unstable*, corresponding to hyperbolic states in the high-dimensional phase space. Currently, there is an intensive search underway for such coherent structures (spatiotemporal patterns) [213, 263, 303, 690, 800] about which chaos is organized. Over a long-time observation of turbulence one expects to see different coherent states in different time intervals. This kind of approach may eventually lead to a periodic-orbit expansion [153] of the chaotic saddle, in full analogy with low-dimensional problems (see Appendix A). There is then hope that the statistical properties of the turbulent flow can be expressed in terms of the properties of the coherent structures.

Finally, we mention that there are other hydrodynamical situations in which the onset of turbulence is similar to that in pipe flows. Notable examples are plane Poiseuille flows (pressure-driven flows between two large parallel plates) [816] and Couette flows (driven by a moving wall) [215, 686, 692]. The common feature in these shear flows is that the laminar profile is stable.[1] One expects therefore in these situations that turbulence is not permanent and decays eventually toward

[1] Plane Poiseuille flows are linearly unstable, but the critical Reynolds number is much above the value at which turbulence transition occurs [217].

a laminar profile. Shear-flow turbulence is thus a case of its own, and is present in the form of high-dimensional chaotic transients. We are thus currently witnessing the appearance of concepts of transient chaos in the study of classical turbulence.

9.7 Closing Remarks

In this chapter we have focused on supertransients. Although they are quite common, there are cases in which the distribution of transient lifetimes is not exponential, or if it is, the average lifetime does not grow rapidly with the system size. It may, e.g., become saturated (for examples, see [252] and [831]). The type of coupling plays an important role [797]. It is, nevertheless, an open question at present whether one can decide from first principles if a system exhibits supertransients. In fact, the question of how to decide whether a spatiotemporal system possesses a chaotic attractor has not been answered. A systematic application of nonlinear stability analysis to different possible asymptotic patterns [517] may provide insights. A recent investigation [813] showed that the master-stability function [583], a central tool in the theory of synchronization in dynamical systems, can successfully be applied as an indicator for transient versus permanent spatiotemporal chaos.

A somewhat analogous phenomenon to supertransients was found in Hamiltonian systems with many degrees of freedom. Any isolated macroscopic system should eventually relax to a state of thermal equilibrium in which any macroscopic variable is independent of time. Nevertheless, in systems with global (mean field) coupling, long relaxations were found whose average time diverges with the number of components [14, 21, 607, 839]. More recently, a metastable state was discovered [531], as characterized by periodic or quasiperiodic oscillations of macroscopic variables about mean values that are different from the respective equilibrium values. The lifetime of the metastable state was found to increase linearly with the number of degrees of freedom. The underlying microscopic dynamics is chaotic, but must have different characters in the metastable and equilibrium states. Both examples can be considered as type-I supertransients, which last long in the thermodynamic limit.

In some spatiotemporal problems the linear size may not be freely chosen. Long transients may, nevertheless, be present (see, e.g., [188, 841]), but it is not apparent whether they scale at all with some parameter of the problem. It is useful to find a scaling parameter in such cases and check whether the dependence is power-law or exponential. In the case of time-delayed systems [841], a natural candidate for some scaling parameter is the delay time.

It is worth pointing out a difference between the shear-turbulence problem and the supertransient phenomena in spatially extended systems other than pipe flows. The scaling in turbulence is not with respect to the length of the pipe, but rather with the diameter D in the Reynolds number. It would be interesting to understand this difference better.

The concept of unstable coherent structures as building blocks for a periodic-orbit type of expansion of the chaotic saddle, or those of the edge of chaos and the invariant sets associated with it, can be applied to all systems exhibiting supertransients. It is quite remarkable that problems ranging from fluid dynamics and chemistry to population dynamics and biology with quite different underlying mathematical structures all share similar features, dominated by long-lasting chaotic transients. A unified understanding of the physics underlying this phenomenon deserves further efforts.